Monitoring Harmonic ELF Magnetic Fields in Data Centers With Sensor-Based Instrumentation

Francisco Portillo, Manuel Fernandez-Ros, Nuria Novas, Rosa Maria Garcia, Eduardo Viciana, and Jose Antonio Gazquez, *Senior Member, IEEE*

***Abstract*—Modern data centers concentrate substantial amounts of power-electronic equipment, generating complex low-frequency electromagnetic environments with implications for electromagnetic compatibility (EMC). This article presents a one-month assessment of the extremely low-frequency (ELF) magnetic field in a data center using an air-core coil magnetometer as a nonintrusive measurement instrument. The sensor operated continuously, and the recorded field was segmented into 5-min windows to compute the root-mean-squared (rms) magnetic flux density (B_{RMS}), the harmonic spectrum from 50 to 2000 Hz, and the total harmonic distortion (THD) of the magnetic field (THD_B). Statistics show moderate field magnitudes, with typical B_{RMS} around 0.5 μT and a maximum below 1 μT, but consistently high-distortion levels, with median THD_B around 36% and occasional values above 300%. Diurnal and weekly analyses reveal that THD_B is strongly modulated by the operating regime, with twice the median distortion during working hours compared with nighttime and weekends, while B_{RMS} varies much less. Harmonic spectra confirm the dominant contribution of low-order odd harmonics, particularly the third, whose relative amplitudes increase under high-distortion conditions. A percentile-based detector identifies 41 high-THD_B events, most of them short-lived (5–10 min). The results illustrate how ELF magnetometry, as a nonintrusive instrumentation approach, can support EMC-oriented characterization of harmonic disturbances in data centers and complement conventional power-quality (PQ) measurements.**

***Index Terms*—Data centers, electromagnetic compatibility (EMC), extremely low-frequency (ELF) magnetometry, harmonic distortion, magnetic field measurement.**

I. Introduction

THE widespread use of power-electronic converters has made low-frequency electromagnetic disturbances a central concern for power-quality (PQ) and electromagnetic compatibility (EMC). Extremely low-frequency (ELF) magnetic fields have gained research focus due to their pervasive nature and potential health implications [1], with recent EMC-oriented work addressing detailed numerical dosimetry and modeling artifacts in low-frequency exposure assessment [2], [3].

Data centers, with their high-powered electronic devices and intricate electrical systems, are critical environments where electromagnetic disturbances affect PQ and EMC, accelerating equipment aging and potentially causing failures or outages [4]. These effects are reflected in the compatibility levels and emission limits defined in IEC 61000 and related standards for public and industrial low-voltage systems.

The expansion of data centers has increased electricity demand [5], [6], with servers and heating, ventilation, and air conditioning being the primary contributors [7]. As information technology (IT) density and power-electronic penetration rise, monitoring electromagnetic disturbances becomes crucial for operators and PQ engineers [8]. Harmonic currents generated by nonlinear loads give rise to distorted voltages and currents, increased losses in transformers and cables, more heating in neutral conductors, and potential maloperation of protection and control devices [9]. These effects are typically described through indices such as total harmonic distortion (THD) and are regulated by international standards on compatibility and emission limits [10]. In data centers, the combined effect of server power supplies, uninterruptible power supplies (UPSs) systems, and other electronic devices generates elevated harmonic levels, especially at odd multiples of the fundamental frequency [11]. Regulatory frameworks such as EN 50160 and IEC 61000-2-4 define compatibility levels for voltage distortion at different points in the supply chain. Still, continuous installation-specific monitoring is often required to verify compliance and to support preventive maintenance.

Conventional PQ assessments in data centers are often conducted with intrusive current and voltage analyzers. As an alternative, ELF magnetic field measurements have been explored to estimate harmonic components and PQ in a noninvasive manner [12], [13], enabling the estimation of fundamental-frequency components, harmonic content, and indirectly PQ indices in a noninvasive manner [14].

Despite the growing importance of data centers, there is a lack of detailed studies on their electromagnetic environments [15], [16]. Information on harmonic signatures and magnetic fields in these centers is limited compared to conventional environments.

In contrast, the present study focuses on a month-long continuous monitoring campaign in an operational data center environment. It develops a long-term characterization workflow for ELF harmonic content and magnetic-domain

Received 24 December 2025; revised 2 March 2026; accepted 27 March 2026. Date of publication 16 April 2026; date of current version 1 May 2026. This work was supported in part by the University of Almeria, the Ministry of Economy, Knowledge, Business and University, and European Regional Development Fund (FEDER) With I + D + I under Project UAL18-TIC-A025-A; in part by the University of Almeria; Andalusian Regional Government through the Electronics, Communications and Telemedicine TIC019 Research Group of the University of Almeria, Spain, under Project P_LANZ_2025/006; and in part by European Union FEDER Program and Research Center for Intensive Mediterranean Agrosystems and Agri-Food Biotechnology (CIAMBITAL) Group. The Associate Editor coordinating the review process was Dr. He Wen. *(Corresponding author: Jose Antonio Gazquez.)*

The authors are with the Department of Engineering, University of Almeria, 04120 La Cañada de San Urbano, Spain (e-mail: portillo@ual.es; mfernandez@ual.es; nnovas@ual.es; rgarciasalvador@ual.es; evg010@ual.es; jgazquez@ual.es).

Digital Object Identifier 10.1109/TIM.2026.3684676

distortion under real operating conditions. This provides a data-driven basis for interpreting harmonic disturbance conditions in modern IT infrastructures and complements conventional PQ assessments when direct electrical instrumentation is unavailable. The main contributions of this work are given as follows.

1) A month-long, continuous monitoring campaign of ELF magnetic field in an operational data center using a nonintrusive air-core coil magnetometer.
2) A distortion-oriented characterization, harmonic spectra, and the magnetic-domain THD, including global, diurnal, and weekly statistics.
3) Regime-based harmonic signatures using normalized harmonic amplitudes.
4) An event-oriented analysis based on a percentile threshold on the magnetic-domain THD to detect and summarize short high-distortion episodes relevant to EMC/PQ supervision.

This article is organized as follows. Section II describes the measurement and processing approach. Section III presents the analysis applied to the data. Section IV discusses implications and limitations. Section V concludes this article.

II. Materials and Methods

A. ELF Magnetometer Setup

The measurements were conducted with the ELF magnetometer previously developed by the authors in the 0–2.2-kHz band [15], [16]. The sensing element is a coreless air-coil with 12 000 turns of 0.25-mm-diameter enameled copper wire. The average coil diameter is 32 cm, and the winding width is 4.5 cm, yielding an inductance of approximately 68.5 H and a self-resonance frequency of about 990 Hz. The coil is configured to measure a single axis of the magnetic flux density (B), which is perpendicular to the sensor area. Preliminary orientation checks indicated that this axis makes the strongest contribution at the installation point and provides a representative estimate of the magnetic field.

The coil output is fed to an analog conditioning stage comprising a low-noise preamplifier, followed by two operational-amplifier-based amplification stages. The conditioned analog signal is digitized by a 24-bit analog-to-digital converter (ADC) that performs oversampling at tens of kilohertz; the embedded digital signal processor (DSP) applies decimation and anti-alias filtering to obtain a final sampling frequency of 4439 samples per second, which defines a usable bandwidth of 2.2 kHz.

The complete measurement chain (air-core coil sensor and analog conditioning stages) was calibrated in the frequency domain by measuring its transfer function using a vector network analyzer, following the same procedure reported in [16]. This calibration is used to correct the amplitude response within the instrument's validated bandwidth. An error analysis based on the manufacturers' specifications of the main analog and conversion components (instrumentation amplifier/op-amp stages and ADC) yields a typical amplitude precision of ±0.63% and a conservative worst case bound of ±4.9% before any corrective measures. The analog conditioning stage

Fig. 1. Location of the sensor inside the data center.

exhibits a noise floor on the order of 10^{-4} nT, which supports that magnetic components in the analyzed band dominate the recorded signals [16].

For this study, the magnetometer was installed in the University of Almeria's data center (Fig. 1), in the main room housing the server racks and associated power-conversion equipment. The monitored facility is a medium-sized data center supplied through a redundant low-voltage distribution system incorporating a 160-kVA APC Symmetra UPS, typically operating at approximately 50% load with occasional higher loading periods. The IT infrastructure consists of 250 heterogeneous servers from different vendors (including HPE, Dell, and Lenovo) with diverse power ratings and utilization patterns. Thermal management is provided by ten APC InRow precision cooling units.

The sensor was positioned at a height comparable to the center of the rack cabinets, and sufficiently far from ferromagnetic structures to avoid local shielding effects. The location was selected to obtain a representative area measurement of the electromagnetic environment while preserving the facility's unobstructed operation. Before the formal monitoring campaign, a brief on-site placement check was performed to select a practical and representative installation point under the room's operational constraints. The subsequent monitoring campaign was conducted at a single fixed location. Since magnetic field magnitudes depend on the conductor and the distance to the current-carrying paths, spatial variability across the room is expected.

B. Data Collection

The monitoring campaign spanned one month of the data center's regular operation (July 2024). During this period, the ELF magnetometer operated continuously and streamed the digitized signal to a dedicated data server over Ethernet.

To capture the full range of operating conditions, the campaign covered working days and weekends, as well as daytime and nighttime periods. No deliberate changes were introduced in the facility; the objective was to characterize the electromagnetic disturbances under routine workload and infrastructure operation. Raw data were stored in binary files, and basic integrity checks (file size and timestamp continuity) were performed before processing to identify and discard corrupt or incomplete records.

C. Harmonic Measurement

The analysis focused on the harmonic content of *B* associated with the 50-Hz main frequency and its harmonics up to 2.2 kHz. Signal processing was performed offline in MATLAB R2024b (The MathWorks, Inc., Natick, MA, USA).

The continuous signal B(t) was segmented into 5-min windows, selected as a compromise between spectral estimation robustness and temporal resolution. This duration is long enough to obtain stable harmonic estimates under quasi-stationary conditions, while still providing minute-scale resolution for analyzing diurnal/weekly patterns and localizing short, high-distortion intervals in long-term monitoring.

For each window, the mean was subtracted to remove any DC offset. The complex spectrum was then obtained by applying the fast Fourier transform (FFT), and the amplitudes of the fundamental component at 50 Hz and the harmonics up to 2.2 kHz were extracted.

The THD of the magnetic flux density (THD_B) was computed for each time window using the standard definition by the following equation:

$$THD_B = \frac{\sqrt{\sum_{h=2}^{hmax} B_h^2}}{B_1} 100\% \quad (1)$$

where B_h is the root-mean-squared (rms) value of the harmonic of order h, B_1 is the rms value of the fundamental component, and h_{max} is the highest harmonic order considered. This definition is analogous to the conventional THD of current or voltage used in PQ assessments and is consistent with the approach adopted in the authors' previous validation studies of the ELF magnetometer [15], [16].

D. Grouping and Analysis

Once the harmonic spectrum and THD_B values were computed for all windows, the results were aggregated to facilitate interpretation in terms of the data center's operating conditions. Time-stamped records were grouped according to hour of the day, day of the week, and broad operational regimes (working hours, night periods, and weekends). For each group, descriptive statistics (median, interquartile range, and selected percentiles) were calculated for both the fundamental component of B and the THD_B.

To characterize the contribution of individual harmonics, the relative amplitudes $|B_h|/B_1$ were computed for each window and harmonic order. Regime-based statistics (median and percentiles of $|B_h|/B_1$ for selected orders) were then derived by pooling all windows within a given regime. This provides a concise description of how the harmonic spectrum changes during working hours, off-hours, and weekends.

High-distortion events were identified by applying a threshold to THD_B. Specifically, the empirical distribution of THD_B was used to determine a percentile-based threshold (the 99th percentile), and contiguous windows with THD_B above this threshold were grouped into single events. For each event, the duration, the range of THD_B, and the corresponding values of $B_{1,\ rms}$ were recorded.

TABLE I
GLOBAL STATISTICS OF B_{RMS} AND THD_B OVER ONE MONTH

	Mean	Median	Std	P05	P95	Max.
B_{RMS} (μT)	0.49	0.51	0.14	0.26	0.72	0.83
THD_B	45.51	35.88	25.33	24.97	95.68	330.90

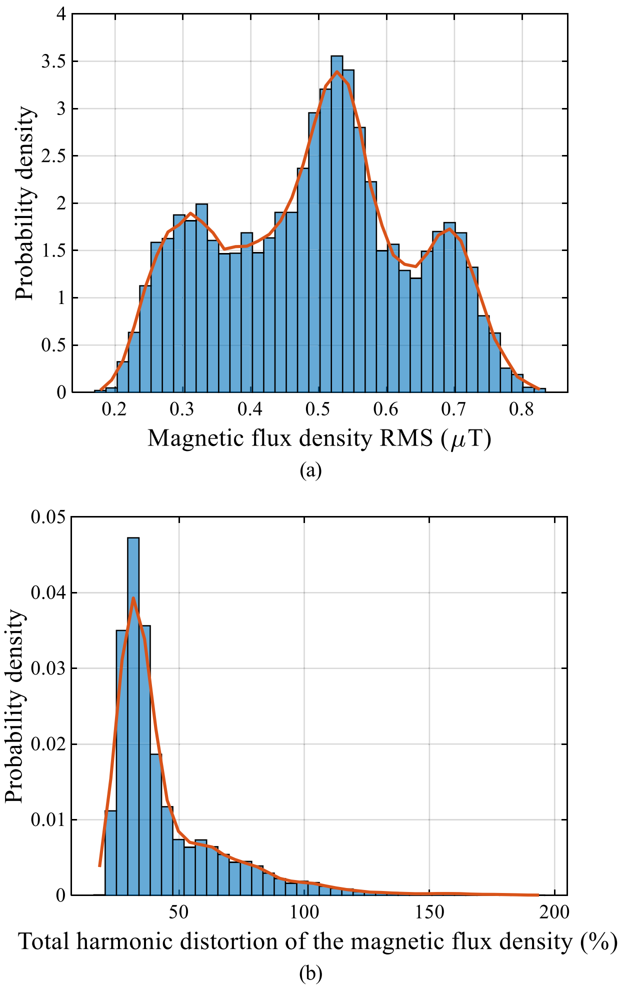

Fig. 2. Probability distributions. (a) B_{RMS}. (b) THD_B.

III. RESULTS

This section presents the results of the one-month monitoring campaign, including global statistics, diurnal and weekly patterns, harmonic spectra, and high-distortion events (referring to time windows in which THD_B exceeds the selected percentile/threshold values), to characterize the electromagnetic environment of the data center and assess the relative severity of its conditions.

A. Overall Magnetic Environment

The one-month monitoring campaign yielded several thousand windows of calibrated magnetic field data, a robust characterization of the electromagnetic environment in the data center. Table I summarizes the global statistics of the rms value of the magnetic flux density (B_{RMS}) and the corresponding THD_B.

TABLE II
PERCENTAGE OF WINDOWS WITH THD_B EXCEEDING GIVEN THRESHOLDS

THD_B threshold (%)	**% time above**
30	76.79
50	26.39
100	4.29

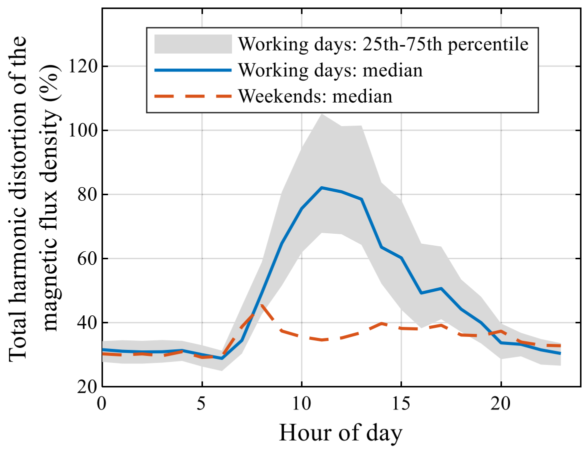

Fig. 3. Typical diurnal profiles of THD_B for working days (solid line and shaded interquartile range) and weekends (dashed line).

Fig. 2 depicts the empirical probability density functions of these two quantities. The distribution of B_{RMS} in Fig. 2(a) exhibits a relatively narrow spread around its typical operating range, with mean and median values near 0.5 μT, a 5th–95th percentile interval of 0.26–0.72 μT, and a maximum below 1 μT. These values show that the magnetic field magnitude remains within a limited range during routine operation. In contrast, THD_B shows a much broader and more skewed distribution [Fig. 2(b)], with the bulk of the probability mass concentrated between 25% and 60%.

To complement these global descriptors, the fraction of windows in which THD_B exceeds selected thresholds (30%, 50%, and 100%) was also evaluated (Table II). These exceedance rates indicate how frequently harmonic distortion reaches levels that may be of concern from a PQ perspective. These exceedance rates motivate the event-oriented analysis reported in Section III-D, in which the timing, duration, and severity of high-distortion intervals are quantified.

B. Diurnal and Weekly Patterns of B and THD_B

The windows collected during the month were next grouped by hour of day and by whether they fell on working days or weekends (Saturday and Sunday). For each category, the median and interquartile range were computed as functions of the hour. Fig. 3 shows the resulting diurnal profiles of THD_B, where the solid line and shaded band correspond to working days and the dashed line corresponds to weekends.

The diurnal pattern of THD_B in Fig. 3 reveals a clear distinction between working days and weekends. On working days, THD_B rises early in the morning, reaches its median peak during business hours, and then decreases in the evening and at night. On weekends, the profile is flatter, with a lower median value and reduced variability over the period.

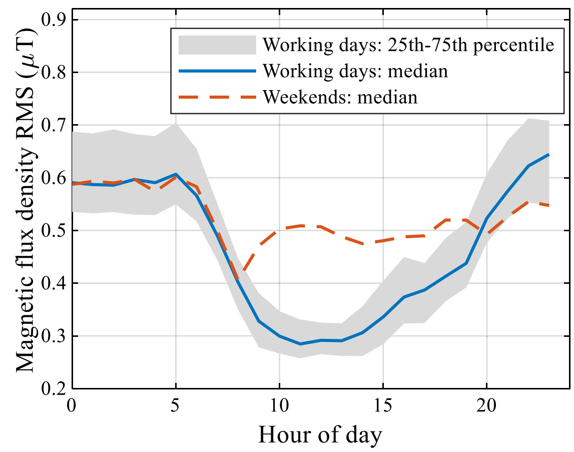

Fig. 4. Typical diurnal profiles of B_{rms} for working days (solid line and shaded interquartile range) and weekends (dashed line).

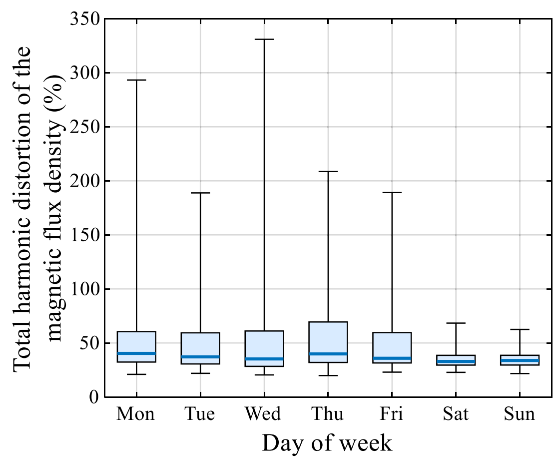

Fig. 5. Day of the week variability of THD_B.

TABLE III
REGIME-BASED STATISTICS

	Median B_{RMS} (μT)	**Median THD_B (%)**	**P95 THD_B (%)**
Working hours	0.32	65.23	126.93
Night/off-hours	0.56	32.17	51.10
Weekends	0.53	33.47	46.65

Fig. 4 presents the corresponding profiles for B_{RMS}. In this case, the variations over the day are smoother than for THD_B. The median B_{RMS} remains within a narrower band, with more modest differences between working days and weekends.

Day-to-day variability in THD_B was further investigated by grouping all windows by day of the week and computing the distribution of THD_B for each day. Fig. 5 shows boxplots of THD_B from Monday to Sunday. The central days of the working week exhibit higher median and wider spreads. In contrast, weekends are characterized by lower central values and narrower interquartile ranges, consistent with lower facility utilization.

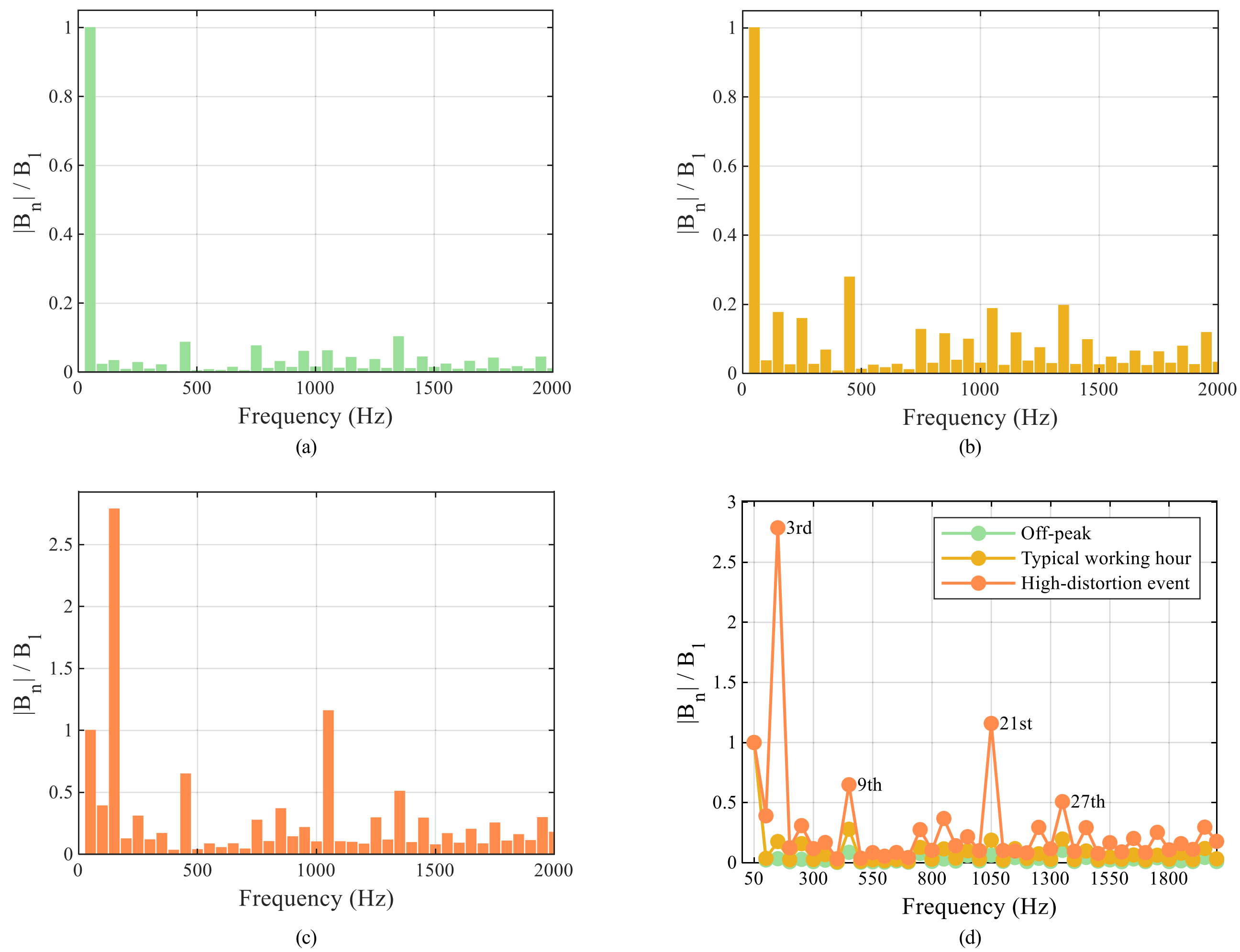

Fig. 6. Relative harmonic content normalizing the rms of each harmonic by the rms of the fundamental component (linear scale) for particular moments. (a) Off-peak (THD_B = 21.7%). (b) Typical working hours (THD_B = 57.0%). (c) High-distortion event (THD_B = 330.9%). (d) Comparison of the harmonic spectrum.

To summarize these patterns, Table III reports regime-based statistics for B_{RMS} and THD_B across three operating regimes: working hours (08:00–18:00), night/off-hours (remaining hours), and weekends. The median THD_B is about 65% during working hours, around 32%–33% during night/off-hours and weekends, and the 95th percentile of THD_B reaches approximately 127% during working hours, compared with about 51% and 47% during night/off-hours and weekends, respectively. In contrast, the median B_{RMS} takes values of 0.32 μT in working hours and around 0.53–0.56 μT in the other regimes.

C. Harmonic Spectrum and Dominant Harmonic Orders

To analyze the spectral composition of the magnetic field under different operating conditions, three representative windows were selected based on their THD_B values: a low-distortion interval with THD_B of the order of 25%, a typical working hour interval with THD_B of the order of 70%, and a high-distortion event with THD_B of 330.9%. For each window, the rms amplitudes of the harmonic bands from 50 to 2000 Hz were computed and normalized by the fundamental component B_1. The resulting relative spectra are shown in Fig. 6(a)–(c) in a linear scale.

In the off-peak case in Fig. 6(a), the fundamental component clearly dominates the spectrum, and the higher order harmonics remain well below 0.2 of B_1. In the typical working hour case in Fig. 6(b), several low-order harmonics (3rd, 5th, 7th, 9th, and 11th) increase in relative amplitude and become clearly visible. In the high-distortion event in Fig. 6(c), the third harmonic exceeds the fundamental in amplitude, and the larger set of odd harmonics, up to around the 20th order, also exhibits elevated levels.

These differences are summarized in Fig. 6(d), which plots, for the three windows, the relative amplitudes $|B_h|/B_1$ as a function of the harmonic order. The comparison highlights the progressive increase in both the magnitude and the spread of the harmonic content as THD_B increases from regular operation to high-distortion conditions.

To characterize the contribution of individual harmonics under different operating regimes, all five windows were grouped into working hours, night/off-hours, and weekends. For each regime and harmonic order between the 3rd and 15th, the median value of $|B_h|/B_1$ was computed.

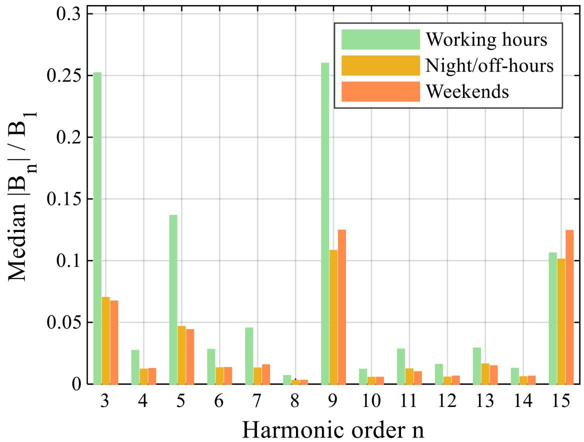

Fig. 7. Typical harmonic levels by operating regime.

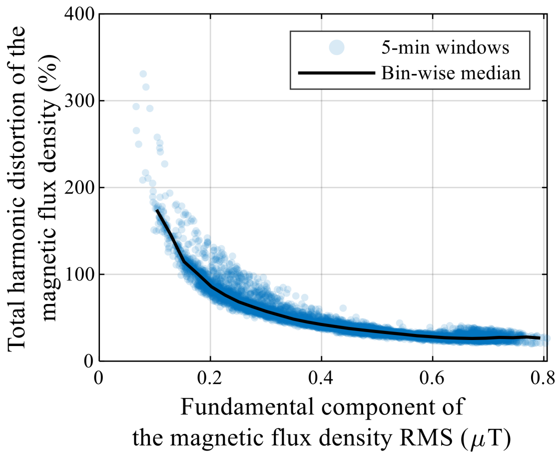

Fig. 8. Relationship between the fundamental component B_{RMS} and THD_B. Each dot corresponds to a window (light blue dots: individual windows; black line: bin-wise median).

Fig. 7 shows the resulting statistics. The 3rd harmonic has the highest median level across all regimes, with $|B_3|/B_1$ approximately 0.25 during working hours and remaining below 0.1 during night/off-hours and weekends. The 5th and 7th harmonics have the next largest median amplitudes, typically in the range 0.03–0.15, depending on the regime. Higher order harmonics above the 11th–13th order exhibit lower median amplitudes, below 0.03 of the fundamental.

Finally, Fig. 8 analyzes the relationship between THD_B and the magnitude of $B_{1,rms}$. Each dot in the scatter plot corresponds to one window of the month-long recording. For each window, $B_{1,rms}$ is computed from the extracted harmonic components, and THD_B is computed as defined previously. The black curve summarizes the central tendency by grouping the data into bins along the $B_{1,rms}$ axis and computing the median THD_B within each bin (bin-wise median). This representation allows the overall trend to be visualized despite the large number of samples and the dispersion of the point cloud. The figure indicates that higher THD_B values are more frequently associated with lower $B_{1,rms}$, suggesting that the most distorted conditions tend to occur when the fundamental component is comparatively small.

TABLE IV
STATISTICS OF HIGH DISTORTION EVENTS

Category	Quantity	Value
Threshold	THD_B threshold (P99) (%)	143.8
Event occurrence	Total number of events	41
	Days with $\geq$ 1 event	11/31
	Events per day (mean $\pm$ std)	1.32 $\pm$ 2.56
	Events per day (min–max)	0-9
Event duration	Duration (min), median (P25–P75)	10.0 (5.0–10.0)
	Duration (min), min–max	5.0–60.0
Levels during events	Max THD_B (%), median (min–max)	168.0 (144.8-330.9)

D. Transient Events Associated With Switching Operations

High-distortion events were identified by applying a threshold equal to the 99th percentile and grouping intervals with THD_B above this threshold into a single event. The resulting statistics are summarized in Table IV.

A total of 41 events were detected during the one-month campaign, occurring on 11 of 31 days and averaging 1.32 $\pm$ 2.56 events per day (range 0–9).

Event durations are typically short, with a median value of 10 min and an interquartile range of 5–10 min, while the minimum and maximum durations are 5 and 60 min, respectively. During these episodes, the maximum THD_B exhibits a median of 168.0%, with values ranging from 144.8% to 330.9%. These figures summarize the frequency and typical duration of high-distortion episodes in the data center.

IV. Discussion

The one-month monitoring campaign in the data center reveals an electromagnetic environment characterized by relatively modest ELF magnetic field magnitudes but systematically high-harmonic distortion. A possible explanation for the lower B_{RMS} observed during working hours is that the monitoring campaign was conducted in July, which corresponds to a vacation period on the university campus. During this period, daytime computational activity in the data center is typically reduced, while routine maintenance and backup operations are frequently scheduled during evening and night hours, contributing to higher net current levels and therefore larger B_{RMS} values outside working hours.

While B_{RMS} remains below 1 μT and exhibits a narrow distribution around a typical value of about 0.5 μT, THD_B is much more variable, with a broad distribution and a long upper tail extending to values above 300%. These levels contrast with previous ELF magnetometer measurements conducted by the authors in an office environment in the same building [16], where similar B_{RMS} magnitudes were accompanied by clearly lower distortion levels (5%–7% during the day and 21%–24% at night). This comparison suggests that, in the data center, power-electronic loads primarily affect the waveform shape rather than the magnetic field amplitude and by extension the underlying currents. Consistent with this interpretation, circuit-level measurements in a real data center reported in [17] show current THD of 75%–83% in lightly loaded branch circuits, despite relatively modest current levels. These results support the view that high-harmonic distortion, combined with moderate field (or current) magnitudes, is a characteristic signature of modern data center loads, especially under partial-load operation. From a measurement perspective, similar environments have motivated the development of dedicated magnetic field instrumentation for EMC applications, such as the portable digital magnetic field meter proposed in [5], which underscores the importance of a wide dynamic range and robust signal conditioning when assessing low-frequency magnetic disturbances. In addition, [18] emphasizes that harmonic currents generated by nonlinear IT power supplies, UPS rectifiers, and variable-speed drives are an intrinsic feature of modern data center infrastructures and that their relative contribution tends to increase under partial-load operation, even when overall power factors remain close to unity. In a related context, [19] analyzed harmonic currents generated by a large computer center in an office building and showed that nonlinear IT loads can produce substantial current distortion at the distribution level, with THD values significantly higher under off-hours and partial-load conditions. Taken together, these results support the view that high-harmonic distortion combined with moderate field (or current) magnitudes is a characteristic signature of contemporary data center loads and has direct implications for both PQ assessment and energy-efficiency analysis.

Furthermore, the diurnal and weekly analyses confirm that the operating regime strongly modulates distortion. During working hours, the median THD_B is roughly twice that observed at night and during weekends, whereas the corresponding changes in B_{RMS} are comparatively small. Similar daily and weekly cycles have been reported in production data centers, where IT and infrastructure energy intensity exhibit clear 24-h and seven-day patterns driven by changes in workload. At the same time, absolute power consumption varies more modestly due to large idle and fixed losses in the supply chain [20]. This pattern is consistent with the expected behavior of a data center, where IT and cooling loads increase during business hours. Still, the supply infrastructure remains dimensioned for the peak load so that the overall current magnitude varies less than the harmonic content. In a related computer-center case study, [19] measured harmonic currents under both working and nonworking hours and between weekdays and weekends, and reported current THD values up to 71% in computer socket circuits, explicitly attributing the wide range of distortion levels to variations in loading and power levels. Furthermore, [18] highlights that nonlinear IT power supplies, UPS rectifiers, and variable-speed drives inherently generate harmonic currents and that for some high-efficiency supplies, harmonic distortion can increase under light-load operation. From a PQ and EMC perspective, this means that periods that are not necessarily associated with the highest currents can still present significantly degraded waveform quality and therefore deserve specific attention in monitoring and mitigation activities.

The spectral analysis clarifies how these distortions arise from the underlying current waveforms. Representative spectra corresponding to off-peak conditions, typical working hours, and a high-distortion event show a progressive reinforcement of low-order odd harmonics, particularly the third, as the THD_B level increases, together with the appearance of additional components at higher orders. Under off-peak conditions, the fundamental clearly dominates, and most harmonics remain well below a few tenths of the fundamental. In contrast, during high-distortion intervals, the 3rd harmonic can exceed the fundamental, and a broad set of odd harmonics up to around the 20th order exhibits elevated relative amplitudes. Regime-based statistics of $|B_h|/B_1$ further indicate that, even under typical operation, several low-order harmonics reach nonnegligible fractions of the fundamental, especially during working hours. Similar spectra, dominated by the 3rd, 5th, and 7th harmonics, have been reported in office computer centers and commercial buildings with large concentrations of switched-mode power supplies and AC drives [21]. These observations are consistent with the expected contributions of UPSs, switched-mode power supplies, and variable-speed drives, and support the use of THD_B as a compact descriptor of waveform degradation in this type of installation. From a PQ and EMC perspective, the predominance of low-order odd harmonics and in particular of the third harmonic is especially relevant in three-phase four-wire distribution systems. Triplen harmonics (3rd, 9th, 15th, ...) are zero-sequence components that add up in the neutral conductor instead of canceling so that high 3rd harmonic currents on each phase can lead to neutral currents well above the phase fundamental, causing overheating of neutral conductors and transformer neutrals and increasing the risk of insulation damage and premature failure [22].

Short-duration events detected using a percentile-based threshold on THD_B provide additional insight into the dynamics of the electromagnetic environment, in line with event-based PQ indices proposed for the detection and classification of disturbance episodes in distribution networks [23], [24]. Although they represent a small fraction of the total monitoring time, the 41 events identified over the month tend to cluster on a limited number of days, with typical durations of 5–10 min and maximum THD_B values well above 140%, reaching approximately 330%.

Because THD_B is defined as a ratio between the rms harmonic content and the rms fundamental component, it is not bounded by 100%. Therefore, very high-THD_B values may occur when $B_{1,rms}$ is comparatively small. In this dataset, the largest THD_B values are observed in windows corresponding to the lower end of the $B_{1,rms}$ range (see Fig. 8), consistent with the behavior of THD-type indices. Such episodes are consistent with disturbance patterns reported for switching operations, changes in UPS operating mode, and other discrete actions in power networks [25]. Even when brief, they can contribute disproportionately to the upper tail of the distortion distribution and may interact with sensitive equipment or protection settings, as highlighted in previous studies on the impact of PQ disturbances on end-user devices and industrial processes [26], [27], [28]. Therefore, they are relevant from an

EMC risk-assessment standpoint and justify the use of event-oriented metrics alongside conventional long-term statistics.

The comparison with a previously monitored office environment in the same building, using the same ELF magnetometer and processing pipeline, helps to place these results in context. While B_{RMS} levels in the data center and in the office are of similar order, the data center systematically exhibits higher THD_B percentiles and greater contributions of low-order odd harmonics. This reflects the higher concentration of power-electronic loads and the different operating profiles of the data center and confirms that, in terms of harmonic distortion, the data center constitutes a more severe electromagnetic environment than conventional office areas supplied from the same low-voltage network.

From a methodological viewpoint, the results illustrate the usefulness of ELF magnetometry as a tool for EMC-oriented characterization of data centers. The nonintrusive nature of the measurement, the ability to operate continuously over long periods, and the possibility of deriving both global indices (B_{RMS} and THD_B) and detailed harmonic patterns from a single sensor make this approach attractive as a complement to conventional PQ analyzers installed at electrical panels. In this context, recent advances in magnetic field measurement circuits, such as the spinning-current-based architectures discussed in [7], underscore the importance of noise and offset mitigation strategies for reliable low-amplitude field measurements in complex electromagnetic environments.

At the same time, several limitations must be acknowledged. The present study is based on a single monitoring point and a single facility, so the spatial variability of the magnetic field and the generalizability of the results are not fully captured. Moreover, the indirect nature of the measurement prevents the direct attribution of specific spectral features to individual feeders or loads without additional information from the electrical installation or from synchronized current and voltage. Regarding the frequency range, the present monitoring campaign characterizes main-related harmonic components in the 50–2000-Hz range, which covers the traditional low-order harmonic range used in many PQ assessments (IEC 61000-3-2). However, modern IT and power-electronic equipment may produce relevant spectral content in the 2–9-kHz range (IEC 61000-4-7). Since the usable bandwidth of the current ELF magnetometer chain constrains the analysis to the range reported in this article, emissions above 2.2 kHz are outside the scope of the results.

Future work should extend the monitoring to multiple locations and axes to distinguish types of data centers, combine ELF magnetometry with conventional PQ instrumentation and operational logs, and investigate automated classification of operating regimes and events based on magnetic signatures. In addition, our research group is actively working to extend the sensing and acquisition chain and its calibration procedures to cover this higher frequency range in future campaigns reliably. Such developments would strengthen the link between nonintrusive field measurements and actionable EMC decisions. They could support the design of monitoring schemes and tailored mitigation measures for the specific harmonic patterns of critical IT infrastructures.

V. Conclusion

This article presents a one-month assessment of magnetic field disturbances in a university data center using a nonintrusive ELF magnetometer. By continuously recording the vertical magnetic field component and processing the data in 5-min windows, the study derived the B_{RMS}, the harmonic spectrum from 50 to 2000 Hz, and the THD_B.

The measurements show that the magnetic field magnitude at the sensor location is moderate, with B_{RMS} typically around 0.5 μT and consistently below 1 μT, whereas the associated distortion is systematically high. THD_B exhibits a broad distribution with median values around 36% and occasional episodes exceeding 300%. Diurnal and weekly analyses indicate that the operating regime strongly modulates distortion. During working hours, the median THD_B is approximately twice that observed at night and during weekends, while B_{RMS} varies much less. Harmonic spectrum and regime-based statistics reveal the dominant contribution of low-order odd harmonics (especially, the 3rd) and highlight that their relative amplitudes increase under high-distortion conditions. A percentile-based detector identifies 41 high-THD_B events over the month, most of which are short-lived (5–10 min) but reach substantial distortion levels.

These results characterize the selected installation point; extension to room-wide characterization requires multipoint measurements, so future work will extend this approach to multiple sensors and diverse types of data centers, combine field measurements with electrical and operational data, and explore automated classification of operating regimes and events based on magnetic signatures, to support PQ supervision and EMC decision-making in critical IT infrastructures.

References

[1] T. Wu, R. Peng, L. Zhang, and K. Li, "Editorial: Human exposure to new-emerging electric, magnetic and electromagnetic fields," *Frontiers Public Health*, vol. 10, Apr. 2022, Art. no. 894624, doi: 10.3389/fpubh.2022.894624.

[2] K. Miwa, Y. Suzuki, J. Lan, Y. Diao, and A. Hirata, "A novel method to predict the maximum electric fields in different body parts exposed to uniform low-frequency magnetic field," *IEEE Trans. Electromagn. Compat.*, vol. 63, no. 5, pp. 1640–1648, Oct. 2021, doi: 10.1109/TEMC.2021.3098573.

[3] J. Gomez-Tames, I. Laakso, Y. Haba, A. Hirata, D. Poljak, and K. Yamazaki, "Computational artifacts of the in situ electric field in anatomical models exposed to low-frequency magnetic field," *IEEE Trans. Electromagn. Compat.*, vol. 60, no. 3, pp. 589–597, Jun. 2018, doi: 10.1109/TEMC.2017.2748219.

[4] J. Sutaria, S. Hajizadeh, S. Rönnberg, and A. Krook-Riekkola, "A perspective of energy and power quality of data center on the grid," *IET Conf. Proc.*, vol. 2021, no. 6, pp. 881–885, Nov. 2021, doi: 10.1049/icp.2021.2145.

[5] S. M. Satav and V. Agarwal, "Design and development of a low-cost digital magnetic field meter with wide dynamic range for EMC precompliance measurements and other applications," *IEEE Trans. Instrum. Meas.*, vol. 58, no. 8, pp. 2837–2844, Aug. 2009, doi: 10.1109/TIM.2009.2016367.

[6] S. S. Panwar, M. M. S. Rauthan, and V. Barthwal, "A systematic review on effective energy utilization management strategies in cloud data centers," *J. Cloud Comput.*, vol. 11, no. 1, p. 95, Dec. 2022, doi: 10.1186/s13677-022-00368-5.

[7] V. Mosser, N. Matringe, and Y. Haddab, "A spinning current circuit for Hall measurements down to the nanotesla range," *IEEE Trans. Instrum. Meas.*, vol. 66, no. 4, pp. 637–648, Apr. 2017, doi: 10.1109/TIM.2017.2649858.

[8] V. Zelencic, M. Miletic, K. R. Raguz, D. Sumina, and I. Erceg, "Reduction of current harmonics in data center power system using single-phase shunt active power filter," in *Proc. 46th MIPRO ICT Electron. Conv. (MIPRO)*, May 2023, pp. 265–270, doi: 10.23919/MIPRO57284.2023.10159912.

[9] Z. Hu, Y. Han, A. S. Zalhaf, S. Zhou, E. Zhao, and P. Yang, "Harmonic sources modeling and characterization in modern power systems: A comprehensive overview," *Electric Power Syst. Res.*, vol. 218, May 2023, Art. no. 109234, doi: 10.1016/j.epsr.2023.109234.

[10] A. Arranz-Gimon, A. Zorita-Lamadrid, D. Morinigo-Sotelo, and O. Duque-Perez, "A review of total harmonic distortion factors for the measurement of harmonic and interharmonic pollution in modern power systems," *Energies*, vol. 14, no. 20, p. 6467, Oct. 2021, doi: 10.3390/en14206467.

[11] K. R. Raguz, M. Miletic, V. Zelenicic, D. Sumina, I. Erceg, and Z. Nastasic, "Analysis of current harmonics in data center power system," in *Proc. 45th Jubilee Int. Conv. Inf., Commun. Electron. Technol. (MIPRO)*, May 2022, pp. 153–157, doi: 10.23919/mipro55190.2022.9803460.

[12] C. Suo, K. Cheng, L. Wang, W. Zhang, X. Liu, and J. Zhu, "Non-contact measurement method of phase current based on magnetic field decoupling calculation for three-phase four-core cable," *Electronics*, vol. 12, no. 6, p. 1443, Mar. 2023, doi: 10.3390/electronics12061443.

[13] C. Xu, W. Wang, Y. Shi, K. Li, and M. Hu, "A noninvasive and self-powered current measurement for power lines based on magnetic field intensity inversion," *IEEE Trans. Instrum. Meas.*, vol. 74, pp. 1–10, 2025, doi: 10.1109/TIM.2025.3568968.

[14] A. Mujezinović, E. Turajlić, A. Alihodžić, M. M. Dedović, and N. Dautbašić, "Calculation of magnetic flux density harmonics in the vicinity of overhead lines," *Electronics*, vol. 11, no. 4, p. 512, Feb. 2022, doi: 10.3390/electronics11040512.

[15] F. Portillo, A. Alcayde, R. M. García, N. Novas, J. A. Gázquez, and M. Férnadez-Ros, "Grid frequency measurement through a PLHR analysis obtained from an ELF magnetometer," *Sensors*, vol. 22, no. 8, p. 2954, Apr. 2022, doi: 10.3390/s22082954.

[16] F. Portillo, A. Alcayde, R. M. García, N. Novas, J. A. Gázquez, and M. Fernández-Ros, "Estimation of the total current harmonic distortion using an ELF magnetometer," *Sens. Actuators A, Phys.*, vol. 371, Jun. 2024, Art. no. 115255, doi: 10.1016/j.sna.2024.115255.

[17] N. Rasmussen. (2007). *Harmonic Currents in the Data Center: A Case Study, Schneider Electric, Data Center Science Center*. Accessed: Dec. 13, 2025. [Online]. Available: https://www.apcbj.com/pdf/SADE-5TNRJN_R1_EN.pdf?

[18] T. Hartman, R. Grootjans, N. Moonen, and F. Leferink, "Electromagnetic compatible energy measurements using the orthogonality of nonfundamental power components," *IEEE Trans. Electromagn. Compat.*, vol. 63, no. 2, pp. 598–605, Apr. 2021, doi: 10.1109/TEMC.2020.3019974.

[19] C. Obiekezie, R. D. C. Santo, K. Webb, and J. Cosgrave, "Optimized parallel feeder for achieving low magnetic fields in an overhead-feeder-type DC rail system," *IEEE Trans. Electromagn. Compat.*, vol. 60, no. 3, pp. 623–628, Jun. 2018, doi: 10.1109/TEMC.2017.2749684.

[20] J. Pflueger. (2010). *Understanding Data Center Energy Intensity*. Accessed: Dec. 13, 2025. [Online]. Available: https://i.dell.com/sites/doccontent/business/large-business/en/Documents/right-2-Dell-Understanding-Data-Center-Energy-Intensity08122010.pdf

[21] K. Kularbphettong and C. Boonseng, "HPFs filtering solutions for reduced the harmonic current generated by SMPS and AC drive systems," *Energy Rep.*, vol. 6, pp. 648–658, Feb. 2020, doi: 10.1016/j.egyr.2019.11.133.

[22] M. Z. Mohd Radzi, B. Ismail, and M. M. Azizan, "Impact of nonlinear and unbalanced loads on neutral conductors in three-phase systems: Modelling and simulation analysis," *Iranian J. Electr. Electron. Eng.*, vol. 21, no. 2, p. 1, 2025, doi: 10.22068/IJEEE.21.2.3639.

[23] M. D. Borras, J. C. Bravo, and J. C. Montano, "Disturbance ratio for optimal multi-event classification in power distribution networks," *IEEE Trans. Ind. Electron.*, vol. 63, no. 5, pp. 3117–3124, May 2016, doi: 10.1109/TIE.2016.2521615.

[24] M. D. Borrás-Talavera, J. C. Bravo, and C. Álvarez-Arroyo, "Instantaneous disturbance index for power distribution networks," *Sensors*, vol. 21, no. 4, p. 1348, Feb. 2021, doi: 10.3390/s21041348.

[25] D. Granados-Lieberman, R. J. Romero-Troncoso, R. A. Osornio-Rios, A. Garcia-Perez, and E. Cabal-Yepez, "Techniques and methodologies for power quality analysis and disturbances classification in power systems: A review," *IET Gener., Transmiss. Distribution*, vol. 5, no. 4, pp. 519–529, Apr. 2011, doi: 10.1049/iet-gtd.2010.0466.

[26] J. E. Caicedo, D. Agudelo-Martínez, E. Rivas-Trujillo, and J. Meyer, "A systematic review of real-time detection and classification of power quality disturbances," *Protection Control Modern Power Syst.*, vol. 8, no. 1, p. 3, Dec. 2023, doi: 10.1186/s41601-023-00277-y.

[27] R. Igual, C. Medrano, F. J. Arcega, and G. Mantescu, "Integral mathematical model of power quality disturbances," in *Proc. 18th Int. Conf. Harmon. Quality Power (ICHQP)*, May 2018, pp. 1–6, doi: 10.1109/ICHQP.2018.8378902.

[28] I. Monedero, C. Leon, J. Ropero, A. Garcia, J. M. Elena, and J. C. Montano, "Classification of electrical disturbances in real time using neural networks," *IEEE Trans. Power Del.*, vol. 22, no. 3, pp. 1288–1296, Jul. 2007, doi: 10.1109/TPWRD.2007.899522.